Korean J. Chem. Eng., 40(12), 2892-2905 (2023)
DOI: 10.1007/s11814-023-1431-1

pISSN: 0256-1115
eISSN: 1975-7220

Functionalized three-dimensional iron-based MIL with high adsorption for removing hazardous organics from water

Maryam Allahbakhshi*, Mohammad Mosaferi,†, Niyaz Mohammad Mahmoodi***,†, Hossein Kazemian****, and Hassan Aslani****

*Student Research Committee, Tabriz University of Medical Sciences, Tabriz, Iran
**Health and Environment Research Center, Tabriz University of Medical Sciences, Tabriz, Iran
***Department of Environmental Research, Institute for Color Science and Technology, Tehran, Iran
****Northern Analytical Laboratory Service (NALS), University of Northern British Columbia (UNBC), Canada
(*Received 8 November 2022 • Revised 7 February 2023 • Accepted 16 February 2023*)

Abstract−MIL-53(Fe) as a three-dimensional MIL was prepared with different precursors-to-solvent ratios and denoted as MIL53B and MIL53C. All as-synthesized samples were modified using 3-amino propyl trimethoxy silane (organosilane) for synthesizing MIL53B/NH_2(0.10), MIL53B/NH_2(0.20), MIL53B/NH_2(0.30), MIL53C/NH_2(0.10), MIL53C/NH_2(0.20), and MIL53C/NH_2(0.30), respectively. The XRD, SEM, EDS, and FTIR techniques were used to characterize materials. The adsorption ability of the materials for the adsorption of dye (Direct Red 23) was studied. The effect of operational parameters was evaluated. The kinetics and isotherm of pollutant removal obeyed pseudo-second-order kinetic and the Langmuir models, respectively. The row and modified MIL53B indicated the adsorption capacity of 1,375 and 4,989 mg/g, respectively. The high pollutant removal ability and fast adsorption rate ascertain that the modified MIL53 could be considered as a dye adsorbent and potentially other organic molecules with similar structures from contaminated water.

Keywords: Surface Functionalization, Three Dimensional MIL, High Adsorption, Hazardous Organic, Pollutant Removal

INTRODUCTION

Several chemicals are produced and used in different industries [1-6]. In the last few decades, with the steadily increasing world population and tremendous growth of modern industrial civilization, contaminants are released into the environment. They destroy ecological safety and threaten the health of human beings. Pharmaceuticals, dyes, herbicides/pesticides, heavy metals, etc. are the most common pollutants in industrial effluents and agricultural runoffs, and their discharge into water bodies has resulted in an increasing trend of the coexistence of different toxic pollutants [7-13].

In the adsorption process, several adsorbents such as metal-organic frameworks (MOFs) are used. The MOFs are porous materials with high surface area. They are synthesized using transition metals (clusters) and bridging organic linkers with controllable pore size. These properties distinguish MOFs from common adsorbents such as zeolites, chitin, graphene oxide, etc. MOFs are used as sensors, separation, catalysis, drug delivery, and adsorption [14-21].

The MILs family, especially iron-based MILs as a group of MOFs, have attracted considerable attention for their stability and non-toxicity. The most unique property of MIL-53(Fe) compared with other MILs is the breathing effect [22-26].

The modifications of metal-organic frameworks can considerably enhance pollutant removal ability. Different materials are used for the functionalization and modification of adsorbents. Organosilane is one of the most important treating agents due to its structure. The modifier creates a covalent bond with the raw adsorbent and leads to unique properties [27-33]. The organic contaminant removal ability of different MOFs, including MOF-235 (Congo red) [34], NU-1000 (glyphosate) [35], ZIF-8/$CoFe_2O_4$/GO (malachite green) [36], ZIF-8@GO (Malachite green) [37], ZIF-67 (Congo red) [38], and Sodalite Zeolite Nanoparticle (Direct red 23) [39], was studied in detail.

A literature review indicated that a detailed study on dye adsorption by the modified MIL-53(Fe) adsorbents has not been carried out. Herein, MIL-53(Fe) was synthesized with different precursors-to-solvent ratios, and the surface of the synthesized samples was modified using organosilane. Direct Red 23 (DR23) was studied as a contaminant. To synthesize the MIL-53(Fe), different amounts of precursors and solvents were used and denoted as MIL53B, and MIL53C. Their surfaces were modified with different amounts of the organosilane. Characterization of synthesized materials as adsorbents was investigated by XRD, SEM, EDS, and FTIR techniques. The differences in behavior and ability of the MILs for organic pollutant adsorption were studied. The DR23 removal conditions from water were investigated. Also, contaminant removal kinetics and isotherm models were presented in detail.

EXPERIMENTAL

1. Materials

The $FeCl_3{\cdot}6H_2O$, H_2BDC, $FeCl_3{\cdot}6H_2O$, N,N-dimethyl formamide (DMF, C_3H_7NO), methanol, ethanol, HCl, and NaOH were

†To whom correspondence should be addressed.
E-mail: mosaferim@tbzmed.ac.ir, mahmoodi@icrc.ac.ir, nm_mahmoodi@aut.ac.ir

Table 1. The synthesis condition of MILs-(Fe)

MOF	H_2BDC (g)	$FeCl_3$ (g)	DMF (mL)	T (°C)	t (h)	Reference
MIL53B	0.415	1.100	50	150	15	[40]
MIL53C	0.322	0.540	10	150	15	[41]

Table 2. The surface modification of MILs-53(Fe) by organosilane

MOF	Organosilane (mL)	Modified MOF_S
MIL53B	0.10	MIL53B/NH_2(0.1)
	0.20	MIL53B/NH_2(0.2)
	0.30	MIL53B/NH_2(0.3)
	0.40	MIL53B/NH_2(0.4)
MIL53C	0.10	MIL53C/NH_2(0.1)
	0.20	MIL53C/NH_2(0.2)
	0.30	MIL53C/NH_2(0.3)
	0.40	MIL53C/NH_2(0.4)

obtained from Merck (Germany). The deionized water was supplied using a Milli-Q apparatus. Direct Red 23 as a contaminant was selected. All chemicals in this research were used without any further purification.

2. Synthesis

2-1. MILs-(Fe)

The MILs-(Fe) was synthesized using DMF (Table 1). H_2BDC (0.415 and 0.322 g) and $FeCl_3{\cdot}6H_2O$ (1.100 and 0.540 g) were separately dissolved in DMF (50 and 10 mL) (Table 1). Then, the H_2BDC solution was added to the $FeCl_3$ solution dropwise. It was stirred for further homogenization and heated at 150 °C for 15 h. After cooling, the obtained solid of MIL-53(Fe) was collected and washed using DMF and methanol. The products were dried at 150 °C overnight. The obtained product was denoted as MIL53B, and MIL53C depending on the precursors-to-solvent ratio.

2. Surface Modification

Surface modification was carried out using organosilane (Supplementary file). The precipitates were dried at 60 °C [42]. The surface modification was performed using 0.1, 0.2, 0.3, and 0.4 mL of organosilane (Table 2).

3. Characterization

The surface of the material was investigated by FTIR (Perkin Elmer, USA). X-ray powder diffraction analysis was used to investigate the crystallinity of materials. The morphology of the synthesized materials as adsorbents was presented by SEM (LEO 1455VP). Chemical analysis and dispersion of different elements of synthesized adsorbents were indicated by the EDS technique. The concentration of dye in water was measured using a double-beam spectrophotometer (Perkin Elmer Lambda 25).

4. Adsorption Experiments

Adsorption experiments were carried out to study the removal capacity, ability, and behavior of the synthesized adsorbents. They were done at ambient pressure and temperature. The effects of adsorbent dose, contaminant concentration, and pH were investigated on pollutant removal.

The effect of adsorbent dose on the pollutant adsorption performance was investigated using various adsorbent doses (0.0005, 0.001, 0.0015, and 0.002 g) into 100 mL of contaminant solutions. Then, they were stirred for 60 min. For investigating the effect of the initial pollutant concentration on the removal process, 0.0020 g of raw and modified adsorbent were dispersed in 100 mL of pollutant solution and the initial concentrations were 100, 125, 150, and 175 mg/L. Then, it was stirred for 60 min. To present the effect of pH, 0.0020 g of adsorbents (pristine and modified) were added into 100 mL of 100 mg/L contaminant solutions and the solution pH was adjusted between 2.1 to 8.1 using HCl or NaOH. The obtained mixture was stirred for 60 min.

After the adsorption process, the adsorbent particles were separated from the samples (withdrawn at different time intervals) by centrifugation and the residual pollutant concentration in water was determined using a UV-Vis spectrophotometer. Removal percentage (%) and adsorption capacity (Q_e: mg/g) of the synthesized adsorbents were measured using Eqs. (1) and (2):

$$\text{Removal}\ (\%) = \frac{(C_0 - C_e)}{C_0} \times 100\% \tag{1}$$

$$Q_e = \frac{(C_0 - C_e)V}{m} \tag{2}$$

C_0 and C_e: the pollutant concentration at initial time and equilibrium, V: volume (L), and m: adsorbent dose (g).

RESULTS AND DISCUSSION

1. Characterization

1-1. FTIR

The surface groups of the synthesized materials were studied using FT-IR spectroscopy (Fig. 1). As presented in Fig. 1, the peak at 3000-3600 cm^{-1} was attributed to the stretching vibrations of O-H groups of surface adsorbed water molecules. The range between 1,500 and 1,000 cm^{-1} as a fingerprint zone shows different peaks which were due to the vibrations of the organic linker in the adsorbents frameworks. Two bands at 1,391 and 1,562 cm^{-1} indicate the vibrations of carboxyl groups in a symmetrical (υ_s(C-O)) and asymmetric (υ_{as}(C-O)) mode. It is due to the dicarboxylate bond. The C-H band vibrations of aromatic rings are described with a peak at 747 cm^{-1}. The presence of a peak at 547 cm^{-1} is due to the Fe-O stretching state and can be attributed to the formation of the metal-oxo cluster between the Fe(III) and the carboxylic of the linker [43,44]. After the surface of the adsorbents was modified with an organosilane, two new peaks appeared at 1,009 and 1,099 cm/1 due to the stretching state of Si-O and Si-CH_2-R [45]. In the modified absorbers, there is a peak at 3,429 cm^{-1}, which is caused by the NH_2 stretching of the amine group and overlaps with the stretching vibration of the hydroxyl group.

1-2. SEM and EDS

The morphology of the synthesized metal-organic frameworks

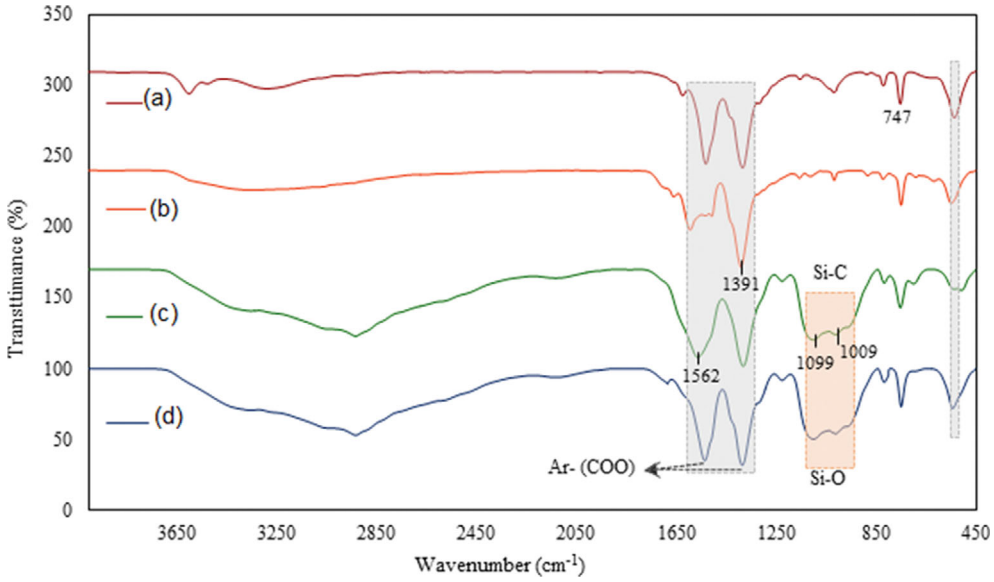

Fig. 1. FTIR spectrum (a) MIL53B, (b) MIL53C, (c) MIL53B/NH_2(0.3), (d) MIL53C/NH_2(0.3).

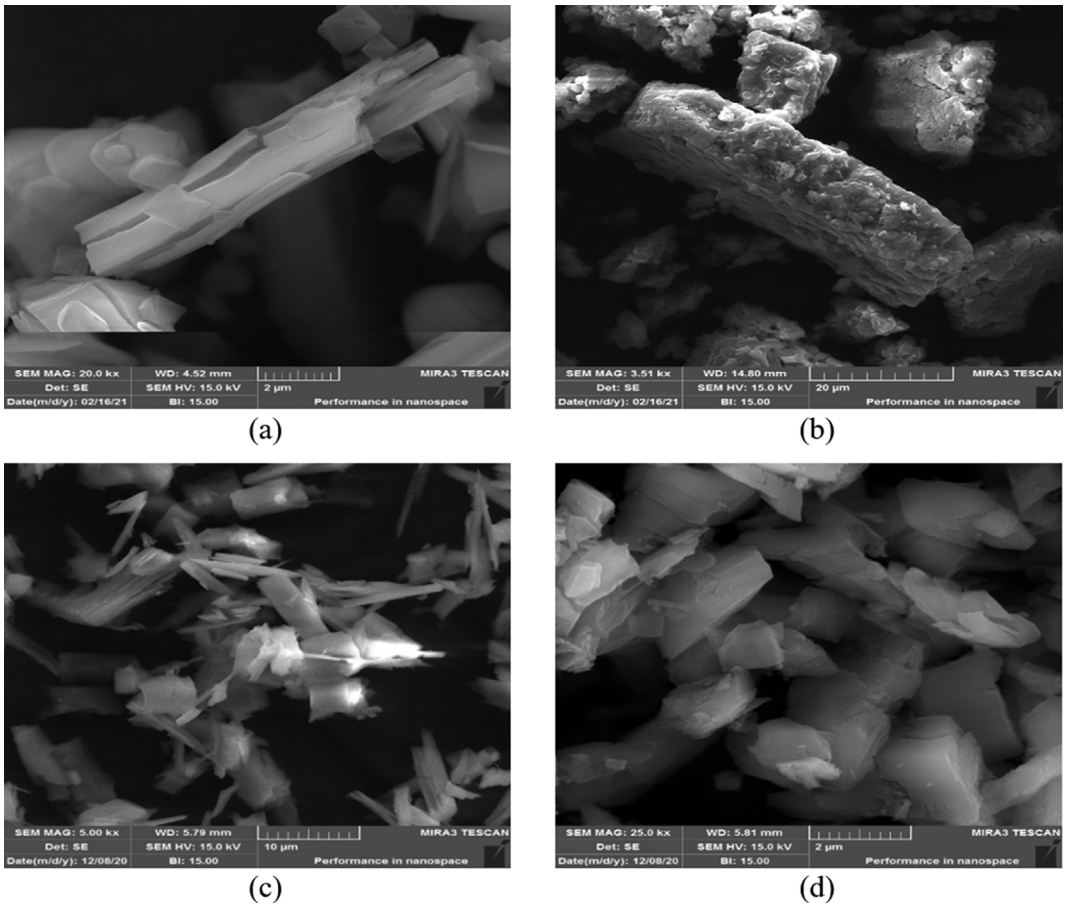

Fig. 2. SEM images (a) MIL53B, (b) MIL53B/NH_2(0.3), (c) MIL53C, and (d) MIL53C/NH_2(0.3).

as adsorbents is shown using SEM images (Fig. 2). As shown in Fig. 2, the MILs-(Fe) were successfully fabricated. It is consistent with the results of previously published works [41,46-48]. It could be observed that MIL53B and MIL53C exhibit different appearance due to the effect of the concentrations of the reactant. From the SEM images (Fig. 2), it is clear that the agglomeration of particles occurred after their modification using the organosilane reagent. This was attributed to the interactions of surface groups in the syn-

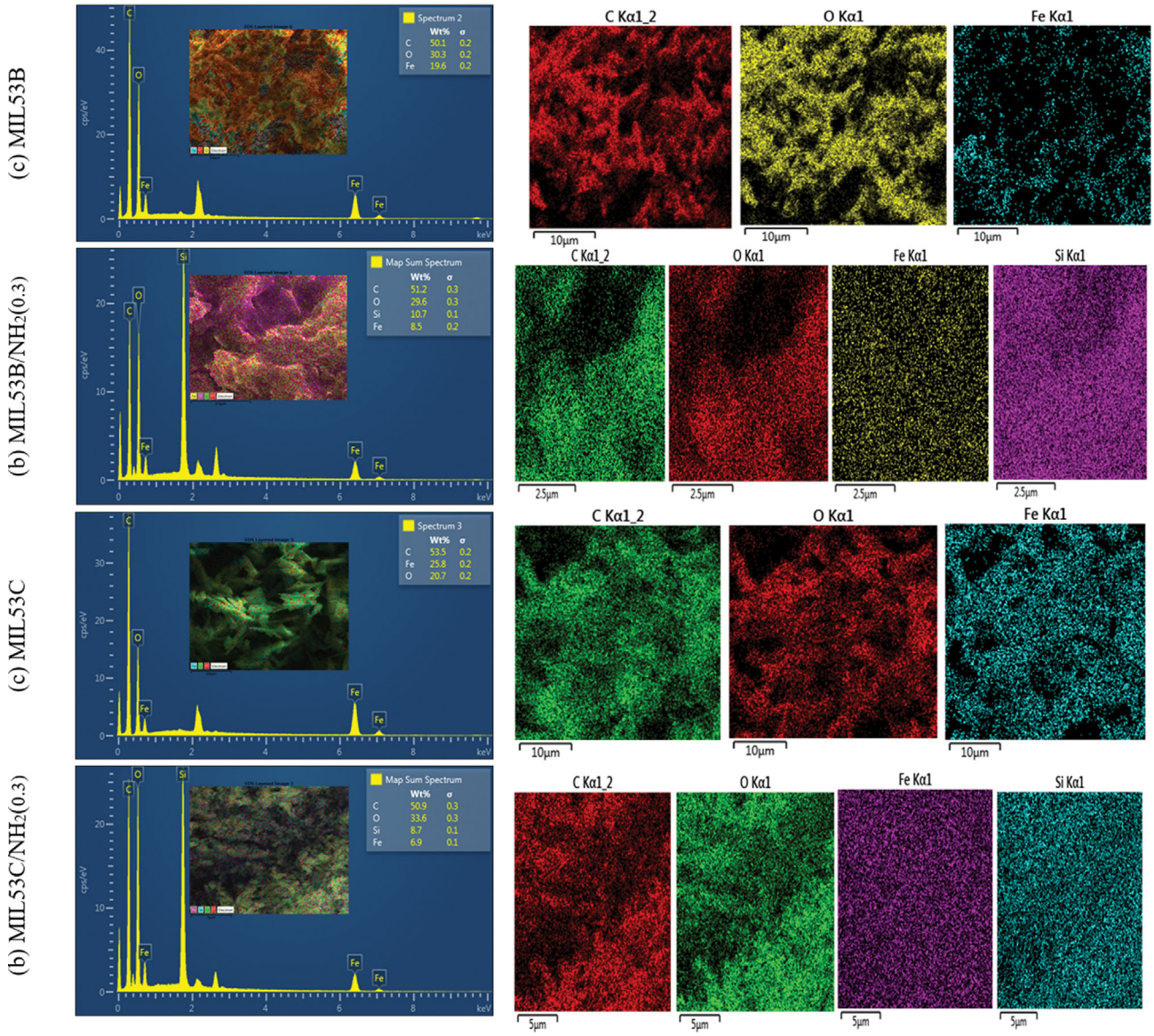

Fig. 3. EDS and surface chemical analysis of different prepared materials (a) MIL53B, (b) MIL53B/NH2(0.3), (c) MIL53C, (d) MIL53B/NH2(0.3).

Table 3. EDS results of the synthesized adsorbents

Element	MIL53B (wt%)	MIL53B/NH_2(0.3) (wt%)	MIL53C (wt%)	MIL53C/NH_2(0.3) (wt%)
C	50.07	51.21	53.47	50.85
O	30.29	29.59	20.68	33.61
Si	-	10.75	-	8.68
Fe	19.64	8.46	25.84	6.86
Total	100.00	100.00	100.00	100.00

thesized MILs as adsorbents.

To study the distribution of different elements in the synthesized MILs structures, EDS analysis was used and indicated in Fig. 3 and Table 3. The data presented C, O, and Fe elements in MIL53B, and MIL53C species. Also, the elemental mapping indicated the homogeneous distribution of these elements in the structure of the adsorbent. In addition, Fig. 3 and Table 3 showed the Si element because of the presence of the silane on the functionalized MILs-(Fe).

1-3. XRD

The XRD patterns of the synthesized MIL53B, and MIL53C

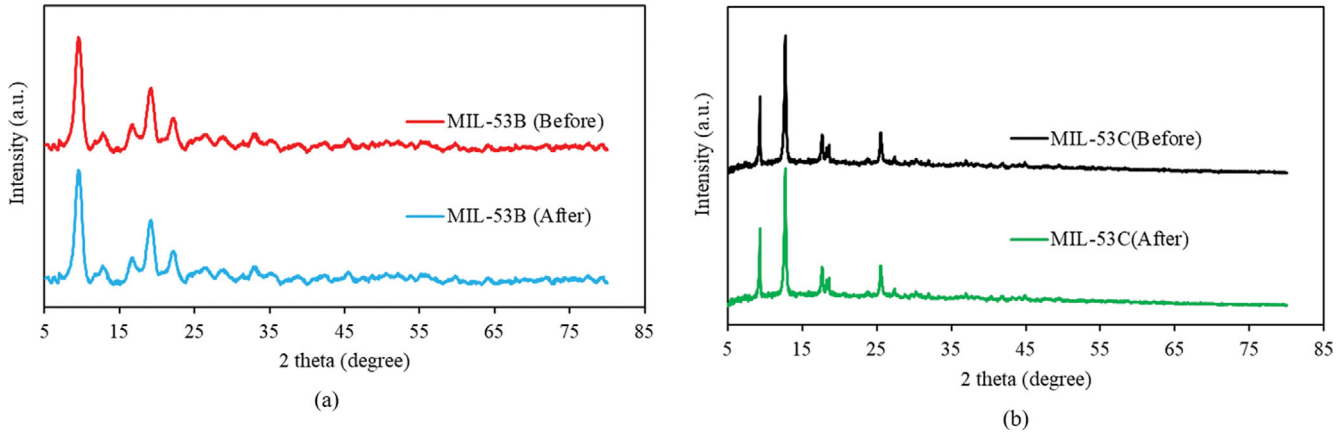

Fig. 4. XRD patterns of MILs before and after pollutant removal process (a) MIL53B and (b) MIL53C.

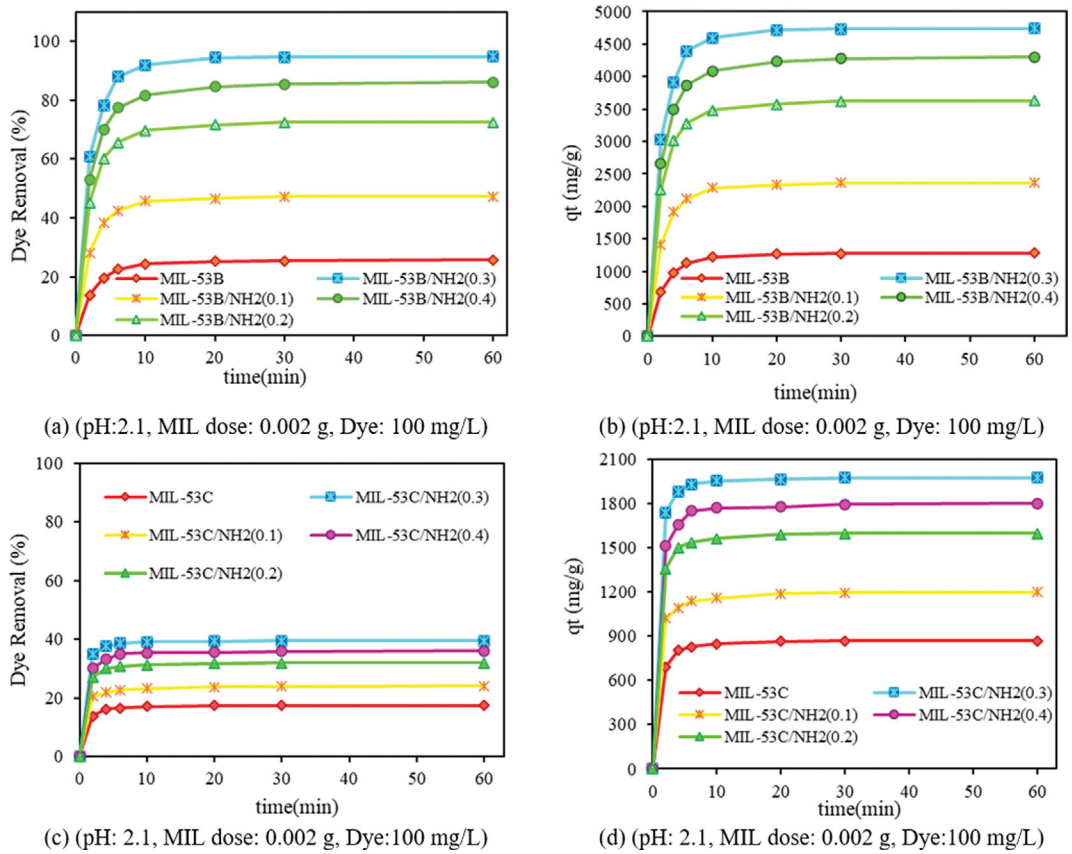

Fig. 5. Effect of organosilane amount on contaminant adsorption ((a) and (c)) and adsorption capacity ((b) and (d)).

(before and after pollutant removal process) are shown in Fig. 4. The XRD patterns of MIL53B and MIL53C followed the previously reported works ([49] and [50], respectively). It could be concluded the successful synthesis of the MILs. Also, Fig. 4 indicates that the XRD patterns of the synthesized MILs after the pollutant adsorption process did not change significantly. It is due to the synthesized adsorbents stability.

2. Contaminant Adsorption

2-1. Adsorbent Modification

The effect of loading the amount of organosilane onto row MILs for adsorbing dye was studied using different values. Experiments were done at different time intervals to investigate the effect of the various ratios on adsorption ability at the same removal conditions (Fig. 5). The results indicated that with organosilane loading (0.1-0.3 ml), the adsorption capacity enhances significantly for all adsorbents. However, the overloading of organosilane (0.4 ml) has an adverse effect on the contaminant adsorption efficiency because of some problems, such as cavity or pore blockage of adsorbents. The obtained data presented the importance of organosilane to remove the dye. The optimum amount of organosilane for MIL53B and

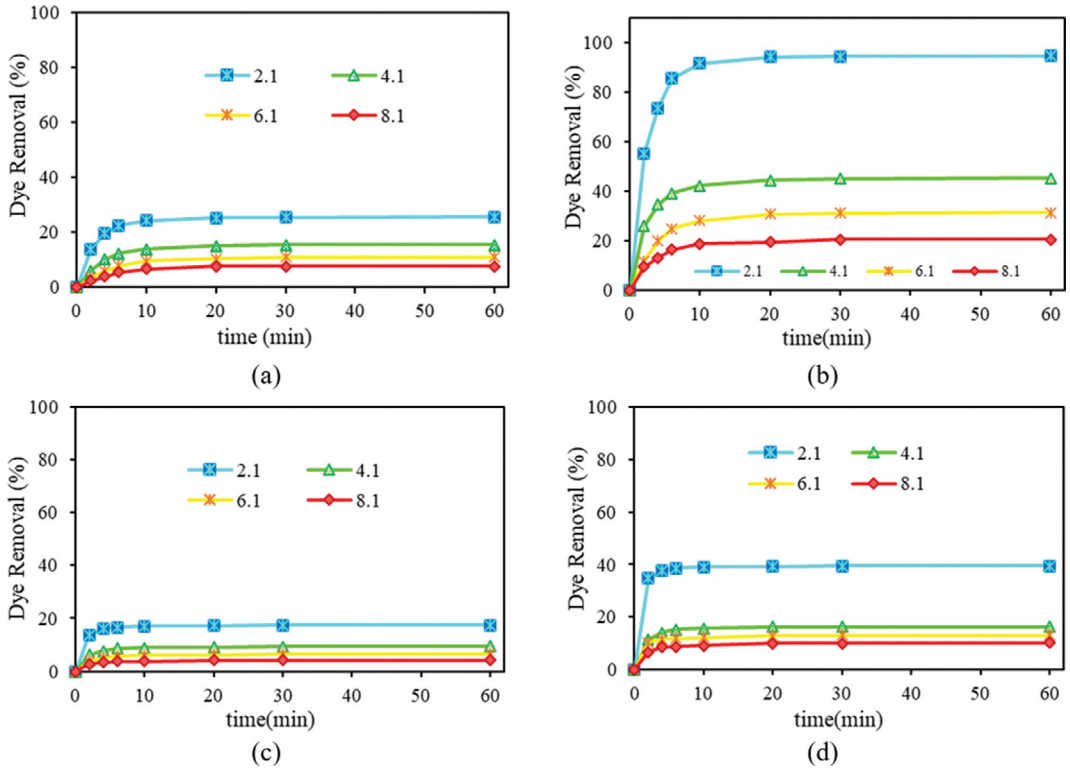

Fig. 6. The pH Effect on the pollutant adsorption (a) MIL53B, (b) MIL53B/NH_2(0.3)), (c) MIL53C, and (d) MIL53C/NH_2(0.3).

MIL53C was 0.3 mL. Thus, it was used for further studies.

2-2. Solution pH

The pH of the solution is a considerable driving force for pollutant removal. It can affect the functional group and the ionization degree of the adsorbates and adsorbents in water and manipulates the contaminant adsorption results [51,52]. Thus, pollutant removal investigation to indicate the solution pH effect on dye removal was carried out at various pH values (2.1, 4.1, 6.1, and 8.1). Fig. 6 presents that the obtained results validating the pollutant removal phenomenon onto adsorbents depends on solution pH. As presented in Fig. 6, the removal curves indicate the same trend for all MILs at various pH values. The data indicate that decreasing the solution from 8.1 to 2.1 considerably enhances the removal ability. It could be attributed that the positive charge density on the surface of adsorbents enhances at acidic pH to remove anionic DR23. Also, the "repulsion effect" between pollutant and adsorbent enhanced at high solution pH [53-55]. Thus, the pH=2.1 was used as the optimum pH for further investigations.

2-3. Dose of Adsorbent

The adsorbent dose is an important parameter in the contaminant removal process which determines the pollutant adsorption percentage as well as the water treatment economics [54]. Thus, the effect of the adsorbent dosage on pollutant adsorption using various doses was studied, while all other adsorption parameters (contaminant concentration, time, and pH) were kept constant. Fig. 7 shows the contaminant removal percentage at different adsorbent doses (0.0005, 0.0010, 0.0015, 0.0020, and 0.0030 g). The adsorption data indicate that the enhancement of the adsorbent dose gives rise to precipitous increasing pollutant adsorption ability. The enhancement of dose was presented in the increasing of adsorbent active sites, which increased the access of contaminant to adsorption sites and caused the enhancement in adsorption ability [56]. However, the overloading of adsorbent (0.0030 g) does not have significant effect on the contaminant removal percentage and adsorption efficiency because of some problems such as agglomeration of adsorbent particles. Thus, 0.0020 g of the adsorbent dose was used as the optimum dose for further studies.

2-4. Pollutant Concentration

The contaminant concentration is another important adsorption parameter, which has a significant effect on the pollutant removal ability [57,58]. Herein, it was investigated the MILs as adsorbents to further study the removal process (Supplementary file). Fig. 8 shows the results of the removal process at various contaminant concentrations: a decrease in adsorption percentage by enhancing the dye concentration. The active sites are constant at a constant adsorbent dose. Thus, this behavior decreases the contaminant adsorption percentage. Herein, 100 mg/L of dye was the optimum concentration for the MIL53B/NH_2(0.3) at 0.002 g of adsorbent.

2-5. Mechanism of Pollutant Removal

Several mechanisms affect the different adsorption processes (Supplementary file). The electrostatic interaction mechanism has a key role in adsorption to study the removal of organic contaminants using MOFs [59-61]. Pollutant adsorption rate depends on the solution pH. Due to the pH importance for removal ability at acidic pH values, the electrostatic attraction is a potential mechanism to study dye removal in this research. Electrostatic interaction is not the sole adsorption mechanism at higher pH conditions due to the repulsive force. Thus, other mechanisms besides electrostatic interac-

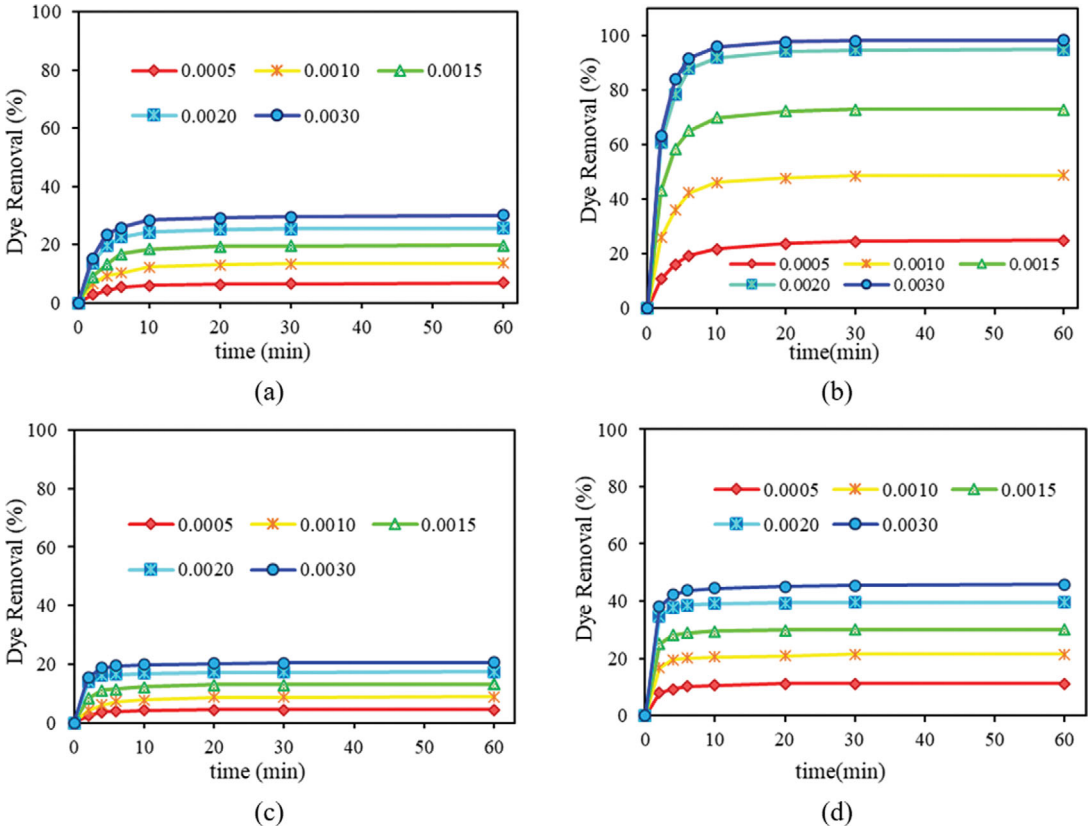

Fig. 7. Effect of adsorbent dose on the dye removal (a) MIL53B, (b) MIL53B/NH_2(0.3)), (c) MIL53C, and (d) MIL53C/NH_2(0.3).

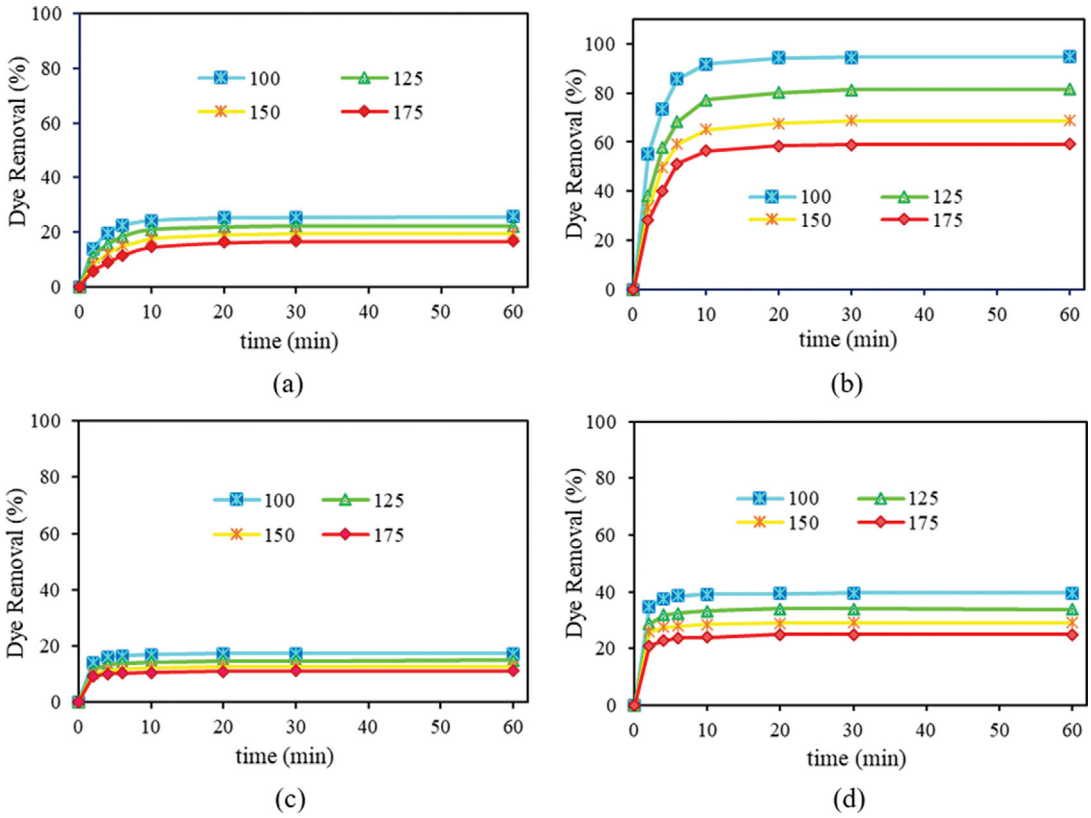

Fig. 8. Initial pollutant concentration effect on dye removal (a) MIL53B, (b) MIL53B/NH_2(0.3)), (c) MIL53C, and (d) MIL53C/NH_2(0.3).

tion affect pollutant removal at higher pH values. The dye aromatic ring interacts with the aromatic ring of the H_2BDC linker of adsorbents by the π-π interactions. In addition, H-bonding is another adsorption mechanism [62,63].

2-6. Adsorption Isotherms

Isotherm models investigate the mechanism of adsorption, the capacity of adsorbent, and the properties of the surface by tracking the adsorbent and adsorbate interaction behavioral trait. There are different isotherm models to interpret and predict adsorption data. In this paper, three models were used. In the Langmuir isotherm, adsorption happens in homogeneously adsorbent active sites with single-layer coverage. Contaminant molecules are adsorbed on specific active surface sites, and each activity site can adsorb only one molecule. The Langmuir model is as Eq. (3) [64,65]:

$$\frac{C_e}{q_e}=\frac{1}{K_l q_l}+\frac{C_e}{q_l} \tag{3}$$

C_e (mg/L): equilibrium concentrations of the solution

K_L (L/mg): Langmuir constant

The Freundlich model indicates the adsorption of organic pollutants with variable affinities on the heterogeneous surface of adsorbent. Its linear equation is as follows [66]:

$$\mathrm{Log}q_e=\log K_F+\frac{1}{n}\log C_e \tag{4}$$

$\frac{1}{n}$: Adsorption intensity

K_F: adsorption capacity per unit concentration

The n value shows adsorption favorability. It is appropriate if n>1.

The Temkin model (Eq. (5)) studies the interplay between the particle of adsorbent and the adsorbed compounds. This model assumes the linearly decreasing heat of adsorption with enhancing the surface coverage [67]. The uniform binding energy distribution occurs in the Temkin model.

$$q_e=\frac{RT}{bT}\ln K_T+\frac{RT}{bT}\ln C_e \tag{5}$$

b_T (kJ/mol): Temkin constant

Isotherm experiments were conducted at pH=2.1 at different amounts of adsorbent (0.0005, 0.0010, 0.0015, 0.0020 g) and 100 mg/L of pollutant concentration. The curves and parameters of the isotherm models that were obtained are shown in Figs. 9-11 and Table 4. The compatibility of isotherm was measured using the value of the correlation coefficient (R^2). The adsorption data followed the Langmuir model with the highest R^2 value. It means that pollutant adsorption forms monolayer coverage of dye on the homogeneous and energetically equivalent active surface sites of MIL.

The contaminant removal capability of MOF-235 (Congo red) [34], NU-1000 [35], ZIF-8/$CoFe_2O_4$/GO (malachite green) [36], ZIF-8@GO (Malachite green) [37], ZIF-67 (Congo red) [38], and Sodalite Zeolite Nanoparticle (Direct red 23) [39] is presented in Table 5. The data indicate that the prepared adsorbents in this research have high adsorption capacity and could be used as superior adsorbents. The surface area of MIL53B and MIL53C was 80 and 52 m^2/g, respectively. MIL53B gained higher amine groups than that of MIL53C by surface modification. Thus, it can adsorb higher pol-

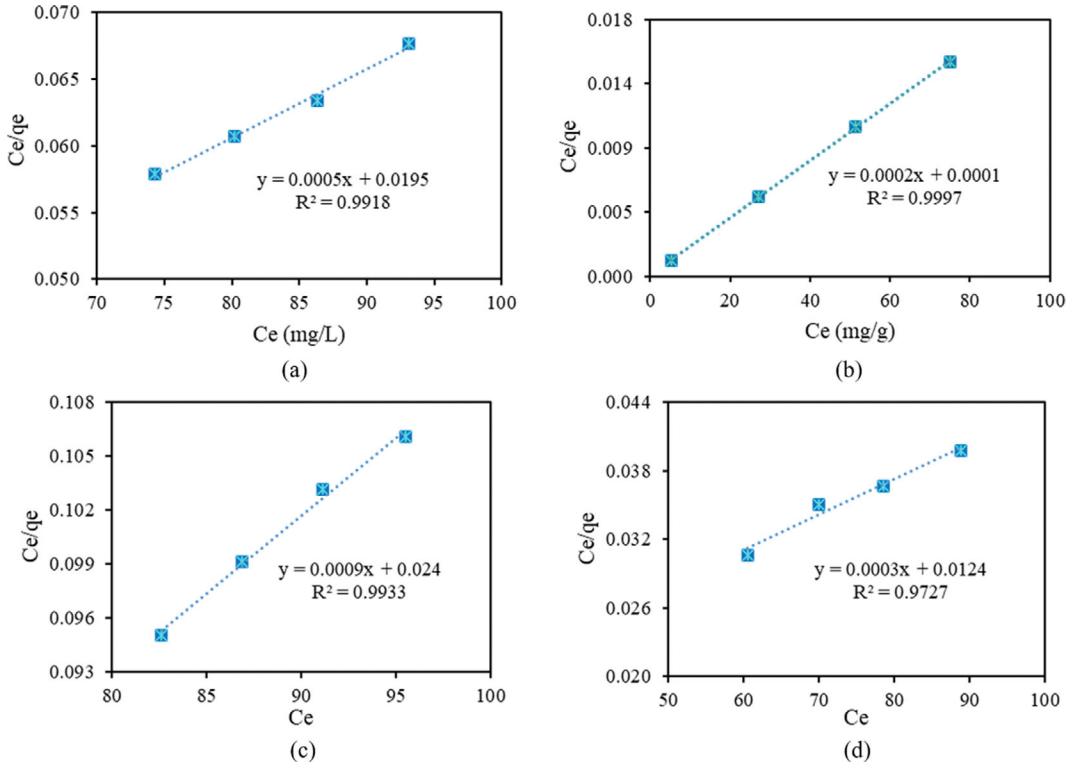

Fig. 9. The Langmuir model (a) MIL53B, (b) MIL53B/NH_2(0.3), (c) MIL53C, and (d) MIL53C/NH_2(0.3).

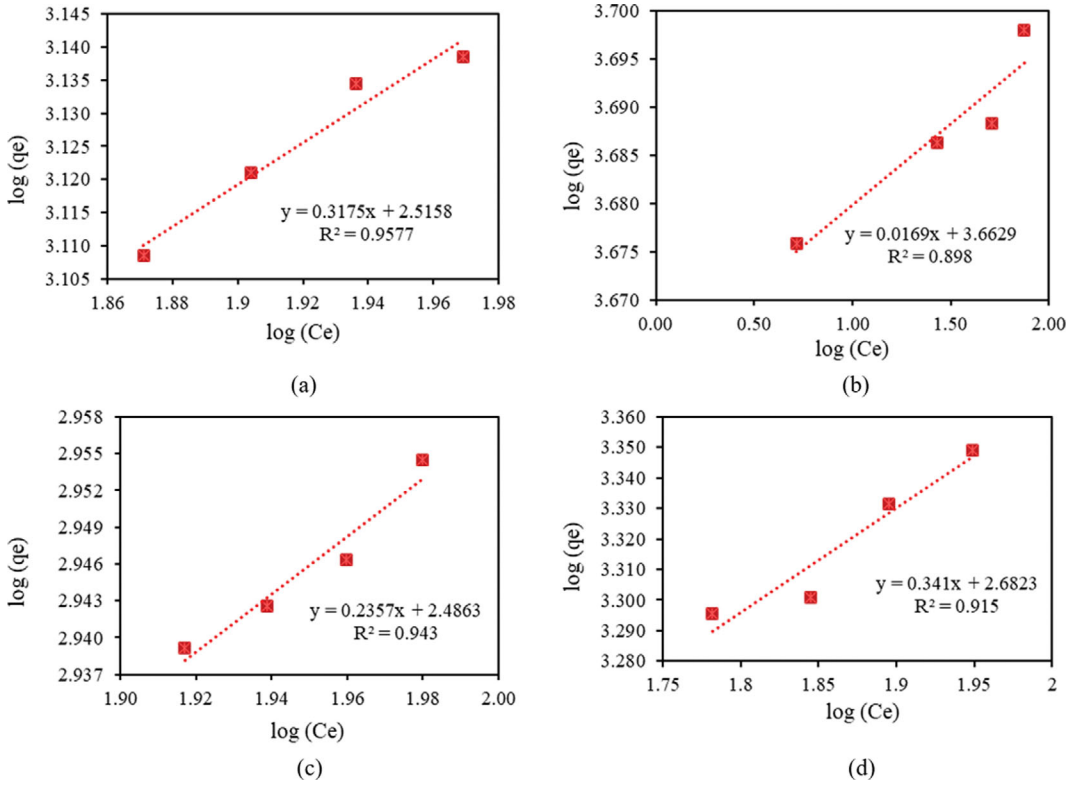

Fig. 10. The Freundlich isotherm (a) MIL53B, (b) MIL53B/NH_2(0.3), (c) MIL53C, and (d) MIL53C/NH_2(0.3).

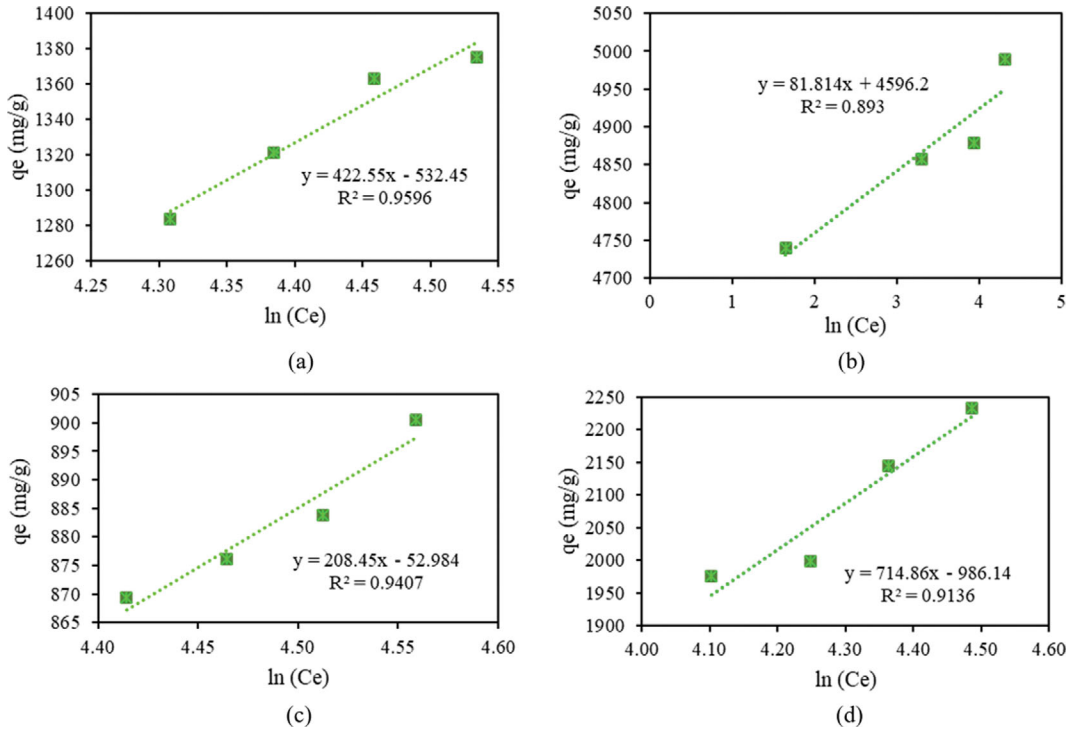

Fig. 11. The Temkin isotherm (a) MIL53B, (b) MIL53B/NH_2(0.3), (c) MIL53C, and (d) MIL53C/NH_2(0.3).

lutant amount.

2-7. Adsorption Kinetics

The kinetic models study the speed of reaction and the reaction rate control. Chemical kinetic depends on different properties of the adsorbates and adsorbents [68,69]. Herein, the kinetics adsorption of dye on the synthesized adsorbents was studied using the

Table 4. The isotherm constants of DR23 removal at various adsorbents amounts

Isotherm	Parameter	Adsorbents	
		MIL53B	MIL53B/NH_2(0.3)
Langmuir $C_e/q_e=1/K_Lq_L+C_e/q_L$	q_L	2,000	5,000
	K_L	0.0256	2.0000
	R^2	0.9918	0.9995
Freundlich $Logq_e=logK_f+1/n\ logC_e$	K_F	327	4,601
	n	3	59
	R^2	0.9577	0.8980
Temkin $q_e=B_1lnk_T+B_1lnC_e$	K_T	8.076×10^5	1.292×10^{-77}
	B_1	−26	−26
	R^2	0.9596	0.8930
		MIL53C	MIL53C/NH_2(0.3)
Langmuir $C_e/q_e=1/K_Lq_L+C_e/q_L$	q_L	1,111	3,333
	K_L	0.0375	0.2419
	R^2	0.9933	0.9727
Freundlich $Logq_e=logK_f+1/n\ logC_e$	K_F	306	481
	n	4	3
	R^2	0.9430	0.9150
Temkin $q_e=B_1lnk_T+B_1lnC_e$	K_T	7.697×10^4	3.139×10^{16}
	B_1	−26	−26
	R^2	0.9407	0.9136

Table 5. The contaminant removal ability of various adsorbents

Adsorbent	Pollutants	Adsorption capacity (mg/g)	Reference
MOF-235	Congo red	1,250	[34]
NU-1000	Glyphosate	1,516	[35]
ZIF-8/$CoFe_2O_4$/GO	Malachite green	2,610	[36]
ZIF-8@GO	Malachite green	3,300	[37]
ZIF-67	Congo red	3,899	[38]
Sodalite zeolite nanoparticle	Direct red 23	4,842	[39]
MIL53C	Direct red 23	900	This research
MIL53C/NH_2(0.1)		1,198	
MIL53C/NH_2(0.2)		1,597	
MIL53C/NH_2(0.3)		2,233	
MIL53B		1,375	
IL-53B/NH_2(0.1)		2,363	
MIL53B/NH_2(0.2)		3,625	
MIL53B/NH_2(0.3)		4,989	

three kinetic models including pseudo-first-order (PFO) [70], pseudo-second-order (PSO) [71], and intraparticle diffusion (IPD) [72]. Figs. 12-14 and Table 6 present the kinetic constants at different adsorbent doses. In PFO, adsorption occurs due to the contaminant concentration gradient between the solution and the surface of the adsorbent. Data indicated that adsorption deviates from the PFO model due to the low R^2 value. The PSO kinetic model relies upon the adsorption capacity. It can predict the adsorption behavior over the whole range of the adsorption process [37]. DR23 adsorption kinetics onto MILs followed PSO kinetic model with a high degree of accuracy for pollutant removal in the studied concentrations and high R^2 values.

The IPD model was also investigated [73]. The linear forms of PFO, PSO, and IPD models are shown as follows, respectively:

$$\mathrm{Log}(q_{eq}-q_t)=\log q_e-\frac{k_{1,\,ad}}{2.303}t \tag{6}$$

$$\frac{t}{q_t}=\frac{1}{k_2q_e^2}+\frac{t}{q_e} \tag{7}$$

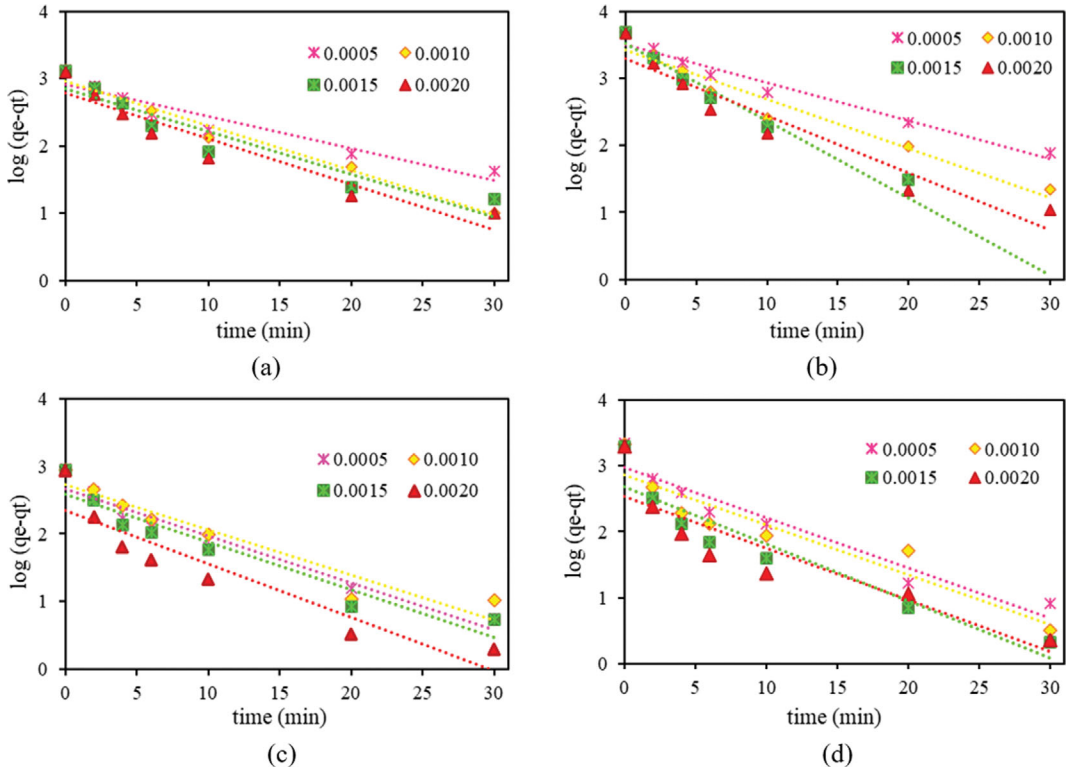

Fig. 12. The PFO kinetic of DR23 removal (a) MIL53B, (b) MIL53B/NH_2(0.3), (c) MIL53C, and (d) MIL53C/NH_2(0.3).

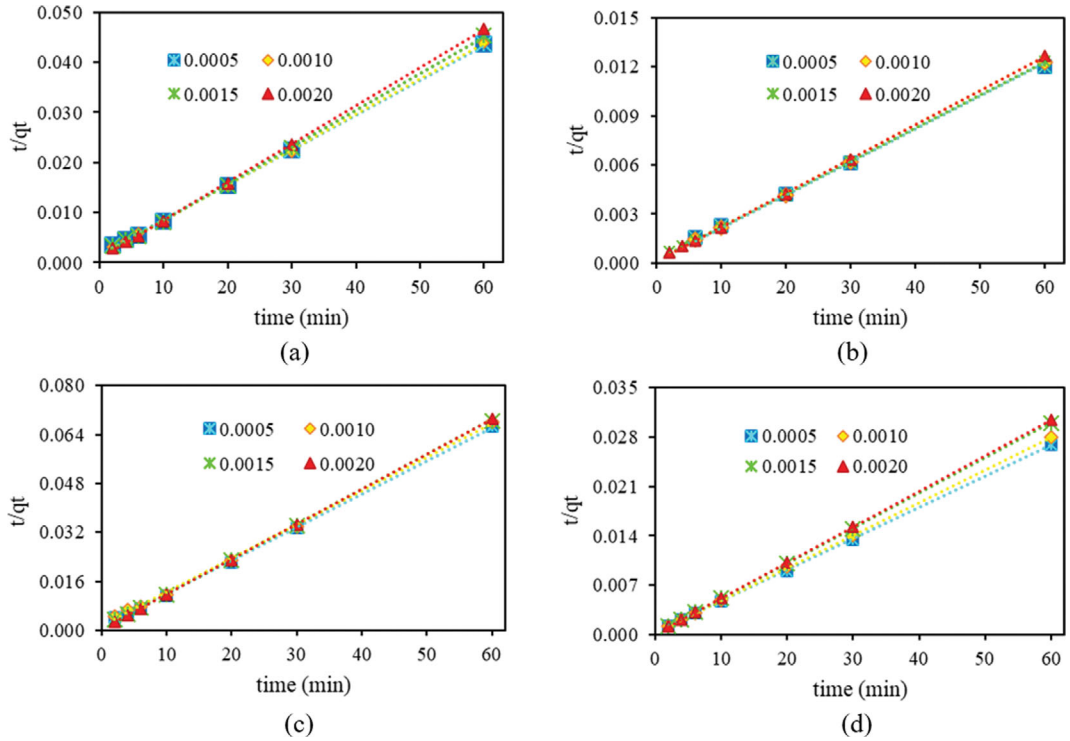

Fig. 13. The PSO kinetic of DR23 removal (a) MIL53B, (b) MIL53B/NH_2(0.3), (c) MIL53C, and (d) MIL53C/NH_2(0.3).

$$q_t = k_p t^{1/2} + I \quad (8)$$

The I=0 presented that the adsorption is solely controlled by the IPD. Thus, the graph of q_t versus $t^{1/2}$ was presented. The results indicate linear regressions with a non-zero I value. The pollutant removal process did not follow the IPD model because the uptake plots did

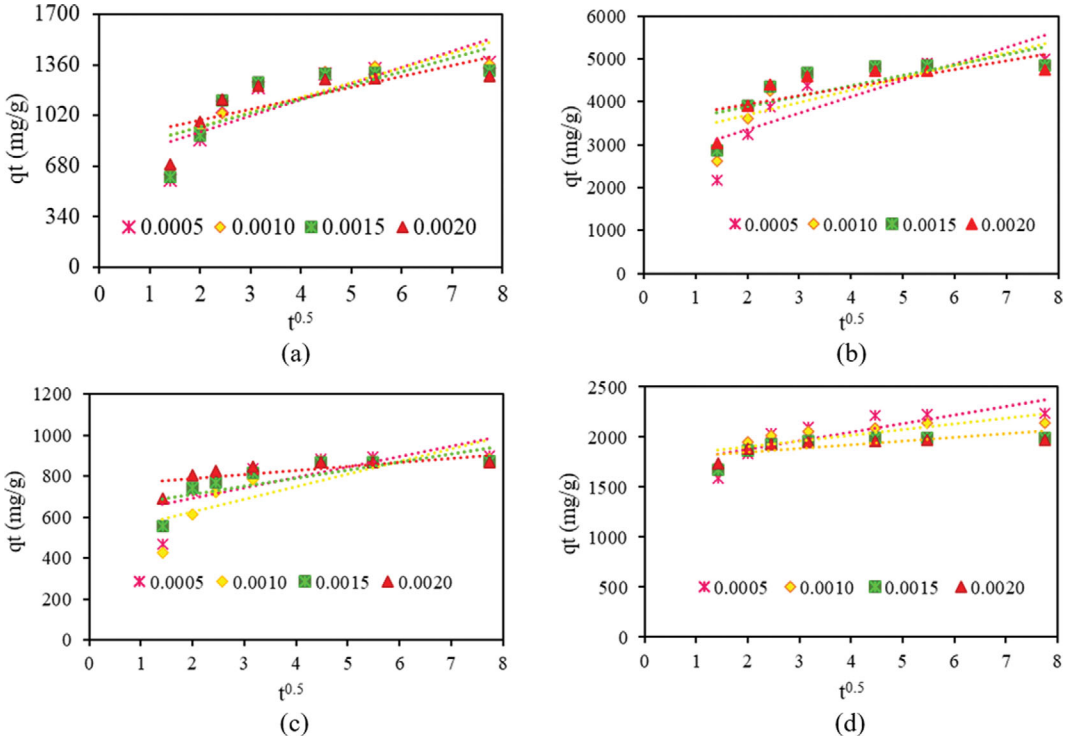

Fig. 14. The IPD kinetic of DR23 removal by (a) MIL53B, (b) MIL53B/NH_2(0.3), (c) MIL53C, and (d) MIL53C/NH_2(0.3).

Table 6. The kinetics constants of DR23 removal at various adsorbent amounts

Adsorbent	Dose (g)	$(q_e)_{Exp}$	Pseudo-first order			Pseudo-second-order			Intraparticle diffusion		
			$\log(q_e-q_t)=\log q_e-(k_1/2.303)*t$			$t/q_t=1/k_2*q_e^2+t/q_e$			$q_t=k_p*t^{0.5}+I$		
			$(q_e)_{Cal.}$	k_1	R^2	$(q_e)_{Cal.}$	k_2	R^2	k_p	I	R^2
MIL53B/NH_2(0.3)	0.0005	4,989	3,228	40	0.9638	5,263	100×10^{-6}	0.9996	386	2,573	0.5882
	0.0010	4,878	2,309	37	0.8879	5,000	133×10^{-6}	0.9997	290	3,120	0.5882
	0.0015	4,856	3,386	20	0.9848	5,000	200×10^{-6}	0.9997	243	3,405	0.5505
	0.0020	4,740	1,964	27	0.9219	4,761	400×10^{-6}	0.9998	204	3,522	0.5241
MIL53B	0.0005	1,375	825	48	0.9164	1,428	306×10^{-6}	0.9997	108	689	0.6930
	0.0010	1,362	911	35	0.9769	1,408	377×10^{-6}	0.9996	98	752	0.7009
	0.0015	1,321	716	36	0.8994	1,369	408×10^{-6}	0.9992	93	755	0.5917
	0.0020	1,283	614	34	0.9092	1,315	711×10^{-6}	0.9997	73	839	0.5690
MIL53C/NH_2(0.3)	0.0005	2,233	941	30	0.9319	2,500	533×10^{-6}	0.9999	87	1,702	0.6471
	0.0010	2,144	720	31	0.8804	2,000	125×10^{-6}	1.0000	57	1,793	0.5808
	0.0015	1,998	480	27	0.8921	2,000	250×10^{-6}	1.0000	38	1,772	0.5216
	0.0020	1,975	340	29	0.8150	2,000	250×10^{-6}	1.0000	27	1,813	0.4988
MIL53C	0.0005	900	461	33	0.9446	909	121×10^{-5}	0.9993	51	633	0.5632
	0.0010	883	528	35	0.9170	909	864×10^{-6}	0.9989	62	547	0.6612
	0.0015	876	383	33	0.9164	909	729×10^{-6}	0.9997	37	690	0.5245
	0.0020	869	224	29	0.8669	909	403×10^{-5}	0.9999	20	770	0.5129

not pass through the origin point. The larger I value is due to a high impact on the boundary layer [74].

2-8. Regeneration

The regeneration ability of adsorbent is an important factor for its practical applications. Thus, the regeneration of synthesized MIL was studied. The results indicate that the recovery efficiency of the MIL did not decrease significantly after three runs of operations. Adsorption ability remains above 75% after the three cycles. Thus, the synthesized MIL not only has high adsorption capacity but also shows good regeneration ability.

CONCLUSIONS

MILs-(Fe) were synthesized with different ratios of precursors-to-solvent and modified with different amounts of the organosilane. Structural characterization verified the successful synthesis of adsorbents. The adsorbents were used to adsorb dye (DR23). The effects of operational parameters on dye adsorption were studied. The data indicated that the contaminant removal is pH-sensitive. Surface modification of the row MILs with organosilane significantly increases their dye removal capacity. The experimental data followed the Langmuir isotherm and PSO kinetics. The row and modified MIL53B showed adsorption capacities of 1,375 and 4,989 mg/g, respectively. It can be concluded that the synthesized organosilane-modified MIL53 adsorbent could be an efficient adsorbent for pollutant removal from water due to its high adsorption capacity, easy regeneration, and reusability.

ACKNOWLEDGEMENT

The research protocol was approved and supported by Student Research Committee, Tabriz University of Medical Sciences (registration code: 99-02-29-64956) (IR.TBZMED.VCR.REC.1399.027).

SUPPORTING INFORMATION

Additional information as noted in the text. This information is available via the Internet at http://www.springer.com/chemistry/journal/11814.

REFERENCES

1. N. M. Mahmoodi, M. Bashiri and S. J. Moeen, *Mater. Res. Bull.*, **47**, 4403 (2012).
2. N. M. Mahmoodi and F. Najafi, *Micropor. Mesopor. Mater.*, **156**, 153 (2012).
3. N. M. Mahmoodi, *Water Air Soil Pollut.*, **224**, 1419 (2013).
4. M. Arami, S. Rahimi, L. Mivehie, F. Mazaheri and N. M. Mahmoodi, *J. Appl. Polym. Sci.*, **106**, 267 (2007).
5. N. M. Mahmoodi, B. Hayati and M. Arami, *Ind. Crops Prod.*, **35**, 295 (2012).
6. K. Gharanjig, M. Arami, H. Bahrami, B. Movassagh, N. M. Mahmoodi and S. Rouhani, *Dyes Pigm.*, **76**, 684 (2008).
7. S. Davarpanah, N. M. Mahmoodi, M. Arami, H. Bahrami and F. Mazaheri, *Appl. Surf. Sci.*, **255**, 4171 (2009).
8. M. Ranjbar-Mohammadi, M. Arami, H. Bahrami, F. Mazaheri and N.M. Mahmoodi, *Colloids Surf. B*, **76**, 397 (2010).
9. N. M. Mahmoodi, *J. Environ. Eng.*, **139**, 1368 (2013).
10. N. M. Mahmoodi, J. Abdi, M. Taghizadeh, A. Taghizadeh, B. Hayati, A. A. Shekarchi and M. Vossoughi, *J. Environ. Manage.*, **233**, 660 (2019).
11. A. Almasian, M. E. Olya and N. M. Mahmoodi, *Fibers Polym.*, **16**, 1925 (2015).
12. D. Asefi, M. Arami, A. A. Sarabi and N. M. Mahmoodi, *Corros. Sci.*, **51**, 1817 (2009).
13. F. Hosseini, S. Sadighian, H. Hosseini-Monfared and N. M. Mahmoodi, *Desalin. Water Treat.*, **57**, 24378 (2016).
14. C. Petit, *Curr. Opin. Chem. Eng.*, **20**, 132 (2018).
15. K. Yu, D. I. Won, W. I. Lee and W. S. Ahn, *Korean J. Chem. Eng.*, **38**, 653 (2021).
16. N. M. Mahmoodi, F. Moghimi, M. Arami and F. Mazaheri, *Fibers Polym.*, **11**, 234 (2010).
17. N. M. Mahmoodi, *Environ. Monit. Assess.*, **186**, 5595 (2014).
18. N. M. Mahmoodi, M. Arami and J. Zhang, *J. Alloys Compd.*, **509**, 4754 (2014).
19. X. Zhang, S. Zhang, G. Ouyang and R. Han, *Korean J. Chem. Eng.*, **39**, 1839 (2022).
20. X.-P. Luo, S.-Y. Fu, Y.-M. Du, J.-Z. Guo and B. Li, *Micropor. Mesopor. Mater.*, **237**, 268 (2017).
21. Z. Luo, J. Li, G. Sui, Y. Zhuang, D. Guo, R. Xu, S. Liang, H. Yao, C. Wang and S. Chen, *Korean J. Chem. Eng.*, **39**, 2127 (2022).
22. Q. Liu, C. Zeng, L. Ai, Z. Hao and J. Jiang, *Appl. Catal. B: Environ.*, **224**, 38 (2018).
23. W. Xiong, Z. Zeng, X. Li, G. Zeng, R. Xiao, Z. Yang, Y. Zhou, C. Zhang, M. Cheng and L. Hu, *Chemosphere*, **210**, 1061 (2018).
24. D. V. Patil, P. B. S. Rallapalli, G. P. Dangi, R. J. Tayade, R. S. Somani and H. C. Bajaj, *Ind. Eng. Chem. Res.*, **50**, 10516 (2011).
25. O. M. Yaghi, M. O'keeffe, N. W. Ockwig, H. K. Chae, M. Eddaoudi and J. Kim, *Nature*, **423**, 705 (2003).
26. Y. Gao, R. Kang, J. Xia, G. Yu and S. Deng, *J. Colloid Interf. Sci.*, **535**, 159 (2019).
27. M. Hasanzadeh, A. Simchi and H. S. Far, *J. Ind. Eng. Chem.*, **81**, 405 (2020).
28. W. Zhang, R.-Z. Zhang, Y. Yin and J.-M. Yang, *J. Mole. Liq.*, **302**, 112616 (2020).
29. J. Yu, W. Xiong, X. Li, Z. Yang, J. Cao, M. Jia, R. Xu and Y. Zhang, *Micropor. Mesopor. Mater.*, **290**, 109642 (2019).
30. Z. Hasan, E.-J. Choi and S. H. Jhung, *Chem. Eng. J.*, **219**, 537 (2013).
31. X. Shang, Y. Zhu and Z. Li, *Appl. Surf. Sci.*, **394**, 169 (2017).
32. P. C. Ma, J.-K. Kim and B. Z. Tang, *Carbon*, **44**, 3232 (2006).
33. S. Wuttke, S. Braig, T. Preiß, A. Zimpel, J. Sicklinger, C. Bellomo, J. O. Rädler and A. M. Vollmar, T. Bein, *Chem. Comm.*, **51**, 15752 (2015).
34. E. Haque, J. W. Jun and S. H. Jhung, *J. Hazard. Mater.*, **185**, 507 (2011).
35. A. Pankajakshan, M. Sinha, A. A. Ojha and S. Mandal, *ACS Omega*, **3**, 7832 (2018).
36. N. M. Mahmoodi, *J. Ind. Eng. Chem.*, **27**, 251 (2015).
37. N. M. Mahmoodi, *J. Taiwan Inst. Chem. Eng.*, **45**, 2008 (2014).
38. Z.-h. Zhang, J.-l. Zhang, J.-m. Liu, Z.-h. Xiong and X. Chen, *Water, Air, Soil Pollut.*, **227**, 1 (2016).
39. O. Tavakoli, V. Goodarzi, M. R. Saeb, N. M. Mahmoodi and R. Borja, *J. Hazard. Mater.*, **334**, 256 (2017).
40. H. Tian, T. Araya, R. Li, Y. Fang and Y. Huang, *Appl. Catal. B: Environ.*, **254**, 371 (2019).
41. W. Dong, L. Yang and Y. Huang, *Talanta*, **167**, 359 (2017).
42. N. M. Mahmoodi, *J. Environ. Eng.*, **139**, 1382 (2013).
43. Q. Zhang, J.-B. Liu, L. Chen, C.-X. Xiao, P. Chen, S. Shen, J.-K. Guo, C.-T. Au and S.-F. Yin, *Appl. Catal. B: Environ.*, **264**, 118529 (2020).
44. T. Araya, M. Jia, J. Yang, P. Zhao, K. Cai, W. Ma and Y. Huang, *Appl. Catal. B: Environ.*, **203**, 768 (2017).
45. O. Medina-Juárez, M. Á. García-Sánchez, U. Arellano-Sánchez, I. Kornhauser-Straus and F. Rojas-González, *Materials*, **9**, 898 (2016).
46. W. Xiong, G. Zeng, Z. Yang, Y. Zhou, C. Zhang, M. Cheng, Y. Liu,

L. Hu, J. Wan and C. Zhou, *Sci. Total Environ.*, **627**, 235 (2018).
47. Q. Wu, Y. Liu, H. Jing, H. Yu, Y. Lu, M. Huo and H. Huo, *Chem. Eng. J.*, **390**, 124615 (2020).
48. C. Zhang, L. Ai and J. Jiang, *J. Mater. Chem. A*, **3**, 3074 (2015).
49. J. O. Hsieh, K. J. Balkus, J. P. Ferraris and I. H. Musselman, *Micropor. Mesopor. Mater.*, **196**, 165 (2014).
50. Y. Zhang, J. Zhou, J. Chen, X. Feng and W. Cai, *J. Hazard. Mater.*, **392**, 122315 (2020).
51. A. B. F. Câmara, R. V. Sales, C. V. dos Santos Júnior, M. A. Fonseca de Souza, C. de Longe, T. M. Chianca, R. D. Possa, L. Carlos Bertolino and L. Santos de Carvalho, *Korean J. Chem. Eng.*, **39**, 1805 (2022).
52. G. Crini and P.-M. Badot, *Prog. Polym. Sci.*, **33**, 399 (2008).
53. T. K. Vo, M. T. Nguyen, V. C. Nguyen and J. Kim, *Korean J. Chem. Eng.*, **39**, 2532 (2022).
54. N. M. Mahmoodi and S. Soltani-Gordefaramarzi, *Prog. Color Colorants Coat.*, **9**, 85 (2016).
55. L. Wu, C. Du, J. He, Z. Yang and H. Li, *J. Hazard. Mater.*, **384**, 121284 (2020).
56. I. F. Nata, D. R. Wicakso, A. Mirwan, C. Irawan, R. Juwita, N. A. Astuti and R. T. An-Nisa, *Korean J. Chem. Eng.*, **39**, 1919 (2022).
57. N. M. Mahmoodi, J. Abdi and D. Bastani, *J. Environ. Health Sci. Eng.*, **12**, 96 (2014).
58. F. Y. Wang, H. Wang and J. W. Ma, *J. Hazard. Mater.*, **177**, 300 (2010).
59. M. Sarker, B. N. Bhadra, P. W. Seo and S. H. Jhung, *J. Hazard. Mater.*, **324**, 131 (2017).
60. B. Hayati, N. M. Mahmoodi and A. Maleki, *Res. Chem. Intermed.*, **41**, 3743 (2015).
61. F. h. Wei, Q. h. Ren, Z. Liang and D. Chen, *ChemistrySelect*, **4**, 5755 (2019).
62. Z. Hasan, N. A. Khan and S. H. Jhung, *Chem. Eng. J.*, **284**, 1406 (2016).
63. P. W. Seo, N. A. Khan and S. H. Jhung, *Chem. Eng. J.*, **315**, 92 (2017).
64. E. R. Alley, *Water quality control handbook*, McGraw-Hill Education (2007).
65. N. M. Mahmoodi and M. Arami, *J. Appl. Polym. Sci.*, **109**, 4043 (2008).
66. N. M. Mahmoodi, *J. Ind. Eng. Chem.*, **20**, 2050 (2015).
67. N. M. Mahmoodi, B. Hayati, H. Bahrami and M. Arami, *J. Appl. Polym. Sci.*, **122**, 1489 (2011).
68. Y. An, H. Zheng, X. Zheng, Q. Sun and Y. Zhou, *J. Hazard. Mater.*, **375**, 138 (2019).
69. B. Hayati, N. M. Mahmoodi, M. Arami and F. Mazaheri, *Clean-Soil, Air, Water*, **39**, 673 (2011).
70. A. Almasian, M. E. Olya and N. M. Mahmoodi, *J. Taiwan Inst. Chem. Eng.*, **49**, 119 (2015).
71. C. Yu, B. Li, K. Zhang, F. Li and H. Yan, *Korean J. Chem. Eng.*, **39**, 198 (2022).
72. Z.-W. Liu, C.-X. Cao and B.-H. Han, *J. Hazard. Mater.*, **367**, 348 (2019).
73. N. M. Mahmoodi, M. Ghezelbash, M. Shabanian, F. Aryanasab and M. R. Saeb, *J. Taiwan Inst. Chem. Eng.*, **81**, 239 (2017).
74. A. Ghosh and G. Das, *Micropor. Mesopor. Mater.*, **297**, 110039 (2020).

Supporting Information

Functionalized three-dimensional iron-based MIL with high adsorption for removing hazardous organics from water

Maryam Allahbakhshi*, Mohammad Mosaferi,†, Niyaz Mohammad Mahmoodi***,†, Hossein Kazemian****, and Hassan Aslani****

*Student Research Committee, Tabriz University of Medical Sciences, Tabriz, Iran
**Health and Environment Research Center, Tabriz University of Medical Sciences, Tabriz, Iran
***Department of Environmental Research, Institute for Color Science and Technology, Tehran, Iran
****Northern Analytical Laboratory Service (NALS), University of Northern British Columbia (UNBC), Canada
(*Received 8 November 2022 • Revised 7 February 2023 • Accepted 16 February 2023*)

2-2. Surface Modification

MIL-53B (1.00 g) was dispersed in water/ethanol. Then, organosilane with different amounts (0.1, 0.2, and 0.3 mL) was added to the solutions and stirred for 24 h. The precipitate was separated and washed with H_2O and dried at 60 °C [42]. The modified samples were denoted as MIL-53B/NH_2(0.1), MIL-53B/NH_2(0.2), and MIL-53B/NH_2(0.3), respectively. The surface modification of MIL-53C was performed by the same process with 0.1, 0.2, 0.3 and 0.4 mL of organosilane (Table 2).

1-1. FTIR

The surface groups of the synthesized materials were studied using FT-IR spectroscopy (Fig. 1). As presented in Fig. 1, the peak at 3,000-3,600 cm^{-1} was attributed to the stretching vibrations of O-H groups of surface adsorbed water molecules. The range between 1,500 and 1,000 cm^{-1} as a fingerprint zone shows different peaks which were because of the vibrations of the organic linker in the adsorbents frameworks. The two sharp peaks at 1,391 and 1,562 cm^{-1} are due to the symmetrical (υ_s(C-O)) and asymmetrical (υ_{as}(C-O)) vibrations of carboxyl groups, respectively. It indicates the presence of the dicarboxylate linker. The band at 747 cm^{-1} is attributed to the vibrations of the C-H bonding of the aromatic rings. Also, a peak at 547 cm^{-1} was due to the Fe-O stretching mode, implying metal-oxo cluster formation between the inorganic metal Fe (III) and the organic linker carboxylic group [43,44]. After surface modification of adsorbents with an organosilane, two new peaks at 1,009 and 1,099 cm^{-1} appeared because of the tensile state of the Si-O and Si-CH_2-R, respectively [45]. The peak at 3,429 cm^{-1} in the modified adsorbents was due to the NH_2 stretch of the amine group which overlaps with the stretching vibration of the hydroxyl group.

2-4. Pollutant Concentration

The contaminant concentration is another important adsorption parameter, which had a significant effect on the pollutant removal ability. Herein, it was investigated for all the MILs to further study the removal process. Fig. 8 showed the obtained data from removal assessment at various contaminant concentrations a decrease in adsorption percentage by enhancing the dye concentration. The number of active sites is constant at a constant adsorbent dose [57]. At higher contaminant concentrations, owing to saturation and lack of required available active points, pollutant molecules in solution face a more difficult fight to find free places on the surface of the adsorbent [58]. Thus, this behavior decreases the contaminant adsorption percentage. Herein, 100 mg/L of dye was the optimum pollutant concentration for MIL53B/NH_2(0.3) at 0.002 g of adsorbent. Thus, it was used for further investigations.

2-5. Mechanism of Pollutant Removal

Several mechanisms affect the different adsorption processes. The electrostatic interaction mechanism has a key role in adsorption to study the removal of organic contaminants using MOFs [59-61]. Pollutant adsorption rate depends on the pH of the solution. Its effect can be studied by taking into account the change in surface charges of both contaminant and adsorbent species at various pH values. The MIL53(Fe) surface has a positive charge under acidic conditions. The amine group (NH_2) of the functionalized MILs protonated to -NH_3^+ at acidic pH conditions and the adsorbent surface becomes positively charged. Thus, the adsorbent positive surface in acidic pH value attracted more anionic molecules. Due to the importance of pH in adsorption ability at a low pH value, electrostatic attraction is a potential mechanism to study dye removal in this research. Electrostatic interaction cannot explain the appreciable adsorption capacity as the sole adsorption mechanism at higher pH conditions because of the repulsive force between the anionic dye and the negative adsorbent surface. Thus, other mechanisms besides electrostatic interaction affect pollutant removal at higher pH values. The π-π stacking has a considerable role in rich electron or electron deficiency systems. The dye aromatic ring interacts with the aromatic ring of the H_2BDC linker of adsorbents via the π-π interactions/stacking. Finally, H-bonding is another adsorption mechanism because of the presence of H-donor and H-acceptor groups in pollutants and adsorbents [52,53].